Food Chemistry 436 (2024) 137703

Contents lists available at ScienceDirect

Food Chemistry

journal homepage: www.elsevier.com/locate/foodchem

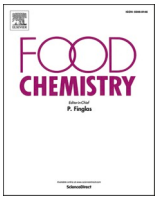

Design of a novel SERS substrate by electrospinning for the detection of thiabendazole in soy-based foods

Mehdi Hajikhani [a], Seyedehalaleh Kousheh [a], Yi Zhang [b], Mengshi Lin [a,*]

[a] Food Science Program, University of Missouri, Columbia, MO 65211, USA
[b] Department of Biomedical Engineering, University of Connecticut, Storrs, CT 06269, USA

ARTICLE INFO

Keywords:
Electrospinning
SERS
Thiabendazole
Detection
Food safety

ABSTRACT

This study aimed to detect and quantify thiabendazole in soy products by surface-enhanced Raman spectroscopy (SERS) coupled with electrospun substrates. Enhanced Raman signals were acquired from uniform electrospun substrates, which were analyzed by focusing on the C=N stretching modes at 1592 cm^{-1} for soy sauce and 1580 cm^{-1} for soy milk. The results revealed a linear relationship between the signal intensity and analyte concentrations with high R^2 values (99.42 % for soy sauce and 99.75 % for soy milk). The limits of quantification (LOQ) were determined to be 69.9 ppb for soy milk and 240.59 ppb for soy sauce samples. The limits of detection (LOD) were found to be 23.1 ppb for soy milk and 79.4 ppb for soy sauce. These findings highlight the effectiveness of the electrospinning-SERS approach for detecting thiabendazole in soy-based food samples, contributing to the understanding of pesticide contamination and ensuring the quality and safety of food products.

1. Introduction

Food contamination is widely considered a major threat to public health (Zheng, Wang, Yuan, & Sun, 2020). Most foods are prone to contamination by various contaminants throughout multiple stages of production, and sometimes even before production. Foods with a delicate nature are at a higher risk of such occurrences (Jallow, Xie, Tang, Qi, & Li, 2021). Both chemical and biological contaminations can cause serious health problems for consumers, including microorganisms (Liu, Galani Yamdeu, Gong, & Orfila, 2020), heavy metals (Hou et al., 2020), chemical waste (Sridhar, Ponnuchamy, Kapoor, & Prabhakar, 2022), herbicides (Xu, Smith, Smith, Wang, & Li, 2019), and pesticides (Umapathi et al., 2021). Each year, millions of people worldwide suffer from various diseases caused by food contamination (Lee & Yoon, 2021). The residue levels of certain contaminants can be extremely low, posing challenges in their detection and identification using conventional methods or requiring expensive equipment (Flores Kim, McCleary, Nwaru, Stoddart, & Sheikh, 2018). Therefore, identifying these contaminants in foods using sensitive techniques is of great importance.

Thiabendazole, a widely used fungicide in agricultural practices, has garnered significant attention due to its potential impact on human health and the environment (Hassan, Xu, Zareef, Li, Rong, & Chen, 2021). As a systemic fungicide, thiabendazole is employed to control fungal diseases and extend the shelf life of various food products. However, its presence in food has raised concerns regarding consumer exposure and potential health risks (Ons, Bylemans, Thevissen, & Cammue, 2020). Soy-based foods were chosen as the focus of this study to identify thiabendazole due to their widespread consumption and importance in various dietary practices. Soy milk and soy sauce, in particular, are commonly used and recognized as key components in vegetarian, vegan, and Asian cuisines, respectively (Qin, Wang, & Luo, 2022). Consequently, through an examination of soy-based foods, the objective of this study is to offer insights into the potential levels of thiabendazole contamination in frequently consumed products, thereby enhancing awareness regarding the potential risks to consumer health (Bajwa & Sandhu, 2014). In recent studies focusing on the identification and measurement of thiabendazole in food samples, several common methods have been employed. These include high-performance liquid chromatography (HPLC), gas chromatography-mass spectrometry (GC-MS), and fluorescence spectroscopy. However, a method that has emerged with notable superiority is surface-enhanced Raman spectroscopy (SERS). Unlike traditional techniques, SERS offers exceptional sensitivity, enabling the detection of trace amounts of analytes with remarkable precision. Additionally, its non-destructive nature, coupled with the ability to provide molecular fingerprinting, ensures minimal sample preparation and a reduced risk of false positives or negatives.

* Corresponding author at: Food Science Program, University of Missouri, Columbia, MO 65211, USA.
E-mail address: linme@missouri.edu (M. Lin).

https://doi.org/10.1016/j.foodchem.2023.137703
Received 25 July 2023; Received in revised form 11 September 2023; Accepted 7 October 2023
Available online 17 October 2023
0308-8146/© 2023 Elsevier Ltd. All rights reserved.

The SERS method not only surpasses the limitations of conventional approaches in terms of sensitivity and selectivity but also holds the potential for rapid, cost-effective, and reliable analysis of thiabendazole in diverse food matrices (Choi et al., 2022).

Raman spectroscopy is a conventional method for identifying contaminants in samples, but this method is not efficient for detecting analytes in very small concentrations, such as parts per billion (ppb) (Petersen, Yu, & Lu, 2021). SERS is an enhanced mode of Raman, which significantly improves the sensitivity of this technology and the limit of detection to enable the identification of analytes down to the ppb level (Wang, Sun, Pu, Wei, & Huang, 2019). For example, porous substrates with a surface functionalized with metal ions can be used in SERS measurement. The substrate needs to have a high specific surface area to enhance the dispersion of the Raman spectrum (Lin & He, 2019). Increasing the specific surface area also leads to a significant increase in the amount of immobilized metal ions on the surface, thereby creating highly reliable signals for detecting various analytes (Logan et al., 2022).

Scaffolds designed using electrospinning are ideal substrates for the SERS method due to their large surface-to-volume ratio (Hajikhani & Lin, 2022). Electrospinning technology is a rapid, user-friendly, and efficient method for producing nanofibers from various polymers (Liao, Loh, Tian, Wang, & Fane, 2018). In this process, a polymer solution is subjected to the influence of a high voltage electromagnetic current, typically around 30 kV. This causes a small jet of polymers, known as a Taylor cone, to spin. The electromagnetic field induces numerous twists and turns in the thin polymer fibers, resulting a reduction in their diameter. Finally, the nanofibers are collected on the opposite side of the device, which is connected to the opposite pole of the electromagnetic current (Hajikhani et al., 2022).

Electrospinning technology offers high flexibility in controlling the morphology of produced nanofibers, which can be tailored to specific applications (Lee, Nishino, Sohn, Lee, & Kim, 2018). Many recent studies have highlighted the positive effect of integrating electrospinning with SERS technology. For instance, in the development of advanced SERS sensors for the identification of microorganisms, substrates designed using electrospinning have significantly improved sensitivity and accuracy in detecting Escherichia coli and Staphylococcus aureus (Yang, Zhang, He, Wang, Zhao, & Sun, 2018). Other studies have successfully utilized electrospun substrates for identifying organic compounds (Singh, Prakash, Misra, Sharma, & Gupta, 2017), pesticides and herbicides (Chamuah et al., 2018; Li, Gu, Feng, Xu, Wang, & Liu, 2020; Shao et al., 2020), and chemical residues (Wan, Zhao, Wang, Zou, Zhao, & Sun, 2021).

The presence of metal ions in the designed SERS substrates is crucial. When incident light interacts with the substrate, it excite local surface plasmon resonances, resulting in an up to 10^6-fold enhancement of the electromagnetic fields through plasmonic coupling (Cong et al., 2015). This magnification can also be attributed to the chemical mechanism that arises from the formation of charge transfer complexes between the absorbed species and the substrate materials, leading to increased electromagnetic fields and intensified Raman signals (Cong et al., 2015). The high specific surface area of electrospun nanofibers provides significant potential for immobilizing metal ions, thereby enhancing the Raman signals (Deng, Liu, Liao, Lin, & Liu, 2019).

However, immobilizing metal ions on the surface of electrospun polymers can be challenging. This problem can be overcome using metal chelating agents that can absorb metal ions from aqueous solutions (Chaúque, Ngila, Ray, & Ndlwana, 2019). One commonly used chelating agent is EDTA, which is known for its capability to remove metal cations typically used in the design of SERS substrates, such as gold, silver, and copper (Chen et al., 2018). This article aimed to investigate the presence of a fungicide thiabendazole in soy-based foods (namely soy milk and soy sauce), which was achieved by developing a highly sensitive and accurate SERS method coupled with the utilization of electrospun nanofibers as SERS substrates to enhance the precision and reliability of the detection (Fig. 1).

2. Materials and methods

2.1. Materials

The following chemicals used in this study were obtained from Sigma-Aldrich (St. Louis, MO, USA), including polyacrylonitrile (PAN) with a molecular weight of 200,000 Daltons, ethylenediamine, gold(III) chloride solution, silver nitrate, L-ascorbic acid, tri-sodium citrate dihydrate, 96 % ethanol, and N,*N*-Dimethylformamide (DMF, 99.8 %). Ethylenediaminetetraacetic acid (EDTA) at 99 % purity was purchased from Acros Organics (Morris Plains, NJ, USA). Triton X-100 and 1-Ethyl-3-(3-dimethylaminopropyl) carbodiimide hydrochloride (EDC) were obtained from ThermoFisher Scientific Inc (Waltham, MA, USA).

2.2. Preparation of nanofibers

The electrospinning of the nanofibers was performed following the protocol described below (Chaúque, Dlamini, Adelodun, Greyling, & Ngila, 2017). Initially, a 10 % PAN solution in DMF was prepared as the polymer solution. The mixture was thoroughly stirred at room temperature for 4 h to ensure complete dissolution. Subsequently, a 0.2 % v/v Triton X-100 surfactant was added to the polymer solution, and the mixing process continued for an additional hour. The resulting polymer solution was then loaded into a polyethylene syringe (18-Gauge needle), which was subsequently positioned inside a syringe pump. Electrospinning was carried out using the NE100 electrospinning/spraying machine (Invenso, Boston, MA, USA). The process parameters, including a flow rate of 1 ml/h, a collector-to-nozzle distance of 20 cm, and a voltage of 10 kV, were kept constant throughout the electrospinning process. The electrospinning process took place under atmospheric pressure and at ambient temperature, with a relative humidity of 75 %.

2.3. Functionalization of nanofibers

- **Amine-Functionalized:** The nanofiber scaffolds were functionalized with amine groups using the following procedure (Chaúque, Dlamini, Adelodun, Greyling, & Catherine Ngila, 2016). The prepared scaffolds were cut into 1 × 1 cm pieces. To initiate the functionalization process, the scaffold pieces were immersed in ethylenediamine for 2 h at 95 °C. The reaction was conducted in an airtight glass container to maintain a controlled environment. Upon completion of the reaction, the scaffold pieces were carefully separated from the reaction environment and rinsed with deionized water three times to remove any residual free crosslinkers. Subsequently, a 100 mM NaCl solution was employed to eliminate any potential electrostatic reactions, and the scaffolds were washed three times with the saline solution. Finally, to remove excess NaCl, the functionalized scaffolds underwent an additional three washes with deionized water. The functionalized scaffolds were then dried at room temperature before further analysis and characterization (Eq. (1).

$$\underset{\text{Polyacrylonitrile}}{R-C\equiv N} + \underset{\text{Ethylenediamine}}{NH_2-C-C-NH_2} \xrightarrow{functionalization} \underset{Amine-Functionalized}{R-C=N-N-C-C-NH_2} \quad (1)$$

- **EDTA-immobilized:** The functionalization of the nanofibers with EDTA was achieved through the following steps (B. Chen et al., 2019; Zhao et al., 2020). Initially, a 100 mM EDTA solution was prepared and treated with EDC crosslinker at a concentration of 200 mM. The

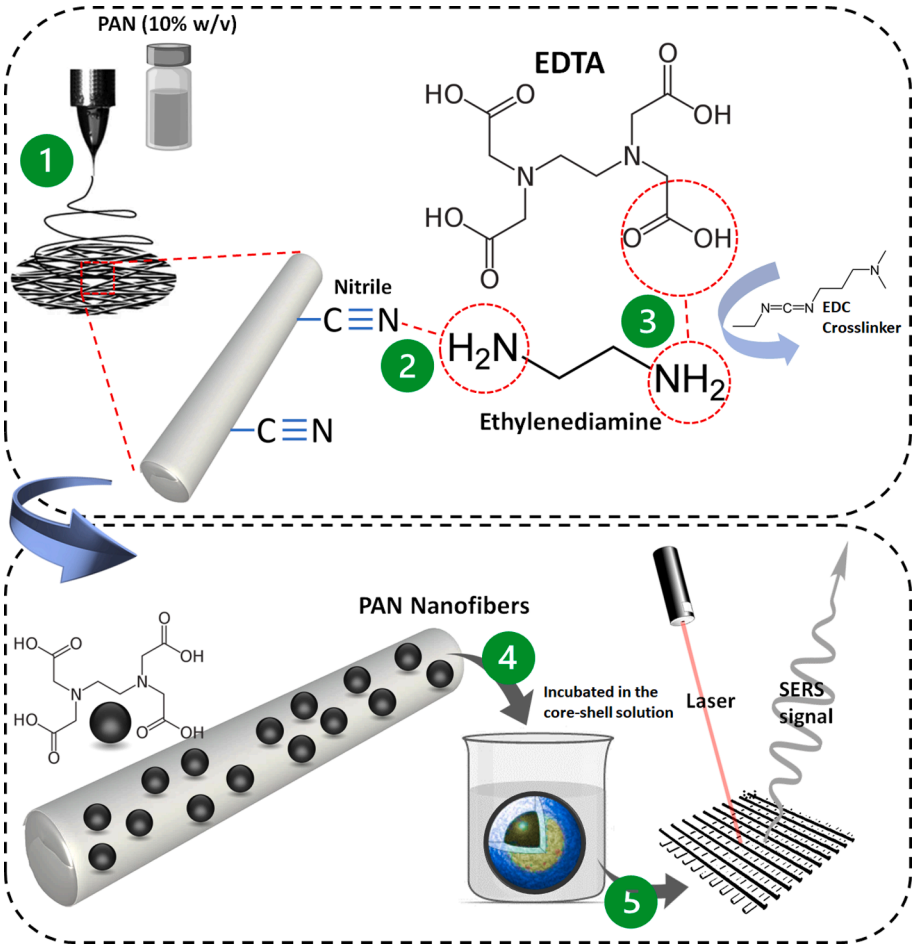

Fig. 1. General schematic of substrate design with the help of surface functionalization of polyacrylonitrile electrospun nanofibers.

activation of carboxyl groups on EDTA was facilitated by conducting the reaction at ambient temperature inside an airtight glass container for 4 h. This activation step ensured that the carboxyl groups were ready to bond with the amine groups present on the surface of the PAN-functionalized nanofibers. Subsequently, the functionalized scaffolds were exposed to an EDTA/EDC reaction solution at a weight/volume ratio of 0.5 %. This reaction was conducted overnight at room temperature within an airtight glass container. Upon completion of the reaction, the scaffolds immobilized with EDTA were carefully separated from the reaction medium. To eliminate any residual chemical residues and mitigate electrostatic interactions, the scaffolds underwent a thorough washing process. Specifically, they were washed three times with deionized water, followed by three washes with a 100 mM NaCl solution, and finally, an additional three washes with deionized water were performed. This comprehensive washing protocol ensured the removal of any unreacted chemicals and minimized potential interference from electrostatic interactions (Eq. (2).

$$\underset{Amine-Functionalized}{R-NH_2} + \underset{\text{Ethylenediaminetetraaceticacid}}{R-(COOH)_4} \overset{immobilization}{\rightarrow} R-NH-C=O-R \underset{EDTA-immobilized}{} + H_2O \quad (2)$$

- **Synthesis of gold-silver core–shell nanoparticles:** The synthesis of gold-silver core–shell nanoparticles was carried out using the following procedure (Asgari et al., 2020). Initially, gold nanoparticles were synthesized by adding 8.6 Âµl of $HAuCl_4$ into 50 ml of deionized water. The solution was heated using a heater stirrer until it reached near-boiling temperature (X. Chen et al., 2019). Subsequently, 1 ml of 1 % tri-sodium citrate dihydrate solution was added, and the solution was maintained at the boiling temperature for 20 min, resulting in a color change to wine red. The solution was then removed from heat and allowed to cool. Next, a 100 mM L-ascorbic acid solution was prepared and mixed with the gold nanoparticle solution at a 1:6 ratio. The mixture was thoroughly stirred for 10 min. Finally, a 1 mM solution of $AgNO_3$ was prepared and slowly added drop by drop to the gold solution while stirring at high speed, at a 1:3.5 ratio. The resulting core–shell nanoparticles were obtained after the addition of the silver solution. These prepared nanoparticles can be stored at refrigerator temperature for up to one week for further use (X. Chen et al., 2019).
- **Coating nanofibers with core–shell nanoparticles:** Coating nanofibers with core–shell nanoparticles was performed using the following methodology (Chaúque et al., 2016; Chaúque et al., 2019). The immobilized scaffolds were immersed in a solution containing core–shell nanoparticles for coating purpose. These scaffolds were introduced into the nanoparticle solution at a weight/volume ratio of 0.05 %. To enhance mass transfer and facilitate the the reaction, a shaker set at a speed of 100 rpm was employed. The coating reaction occurred at room temperature and was allowed to proceed overnight. This extended duration ensured sufficient time for the nanoparticles to adhere and coat the surface of the scaffolds effectively. Following the completion of the nanoparticle coating, the prepared scaffolds were carefully separated from the nanoparticle solution. Subsequently, the scaffolds were air-dried at room temperature. This drying process enabled the firm adhesion of the immobilized core–shell nanoparticles to the nanofiber surface, rendering them

suitable substrates for subsequent analysis and utilization in the SERS measurement.

2.4. Characterization of nanofibers

The characterization of nanofibers was carried out using various techniques to assess their properties and confirm successful functionalization and coating. First, Fourier transform infrared spectroscopy (FTIR) (Nicolet 380, ThermoFisher Scientific Inc.) was employed to detect potential interactions between functional groups present in the nanofibers. This analysis provided insights into the chemical bonding and structural changes resulting from the functionalization process (Yu, Wang, Kong, Lin, & Mustapha, 2019). To examine the macroscopic and morphological features of the nanofibers, transmission electron microscopy (TEM) coupled with energy-dispersive X-ray spectroscopy (EDS) was employed to investigate the core–shell nanoparticles that were coated onto the nanofibers (Spectra 300 STEM, ThermoFisher Scientific Inc.). TEM provided detailed information on the size, shape, and distribution of nanoparticles, while EDS enabled elemental analysis and mapping, confirming the presence of the desired core–shell structure on the nanofibers (Asgari et al., 2020). These characterization techniques provided valuable insights into the functionalization process, morphology, and composition of the nanofibers, validating their suitability for further analysis and applications in the study, particularly concerning the immobilization and characterization of core–shell nanoparticles.

2.5. Identification of analytes in food samples

Soy milk sample: The identification of thiabendazole in soy milk samples was conducted using the following methodology. Initially, specific amounts of thiabendazole were spiked into the soy milk samples to create a known concentration for analysis. To remove proteins from the samples, the pH of the solution was adjusted to 4.5, causing the proteins to precipitate at their isoelectric point. The resulting protein clots were removed by centrifugation at 20,000 g for 2 min, and the supernatant was separated. To further eliminate any remaining proteins and carbohydrates soluble in the serum, 96 % ethanol was added to the supernatant in a volume ratio of 50 %. This mixture was then subjected to an additional centrifugation at 20,000 g for 2 min to remove sediments. The resulting supernatant was used for the identification of thiabendazole. For the identification process, 10 μl of the sample was dropped onto a substrate placed on a gold-coated slide. The sample-loaded substrate was then placed inside a Raman spectrometer after it was dried under ambient conditions, which allowed for the analysis of the sample and the identification of thiabendazole (M. Chen et al., 2022; Li, Teng, Nie, & Liu, 2018).

Soy sauce sample: The identification of thiabendazole in soy sauce samples was conducted using the following procedure. First, specific amounts of thiabendazole were spiked into the soy sauce samples to create known concentrations for analysis. To remove soluble compounds, 96 % ethanol was added to the samples at a volume ratio of 50 %. This mixture was then subjected to centrifugation at 20,000 g for 2 min to separate the sediments, and the resulting supernatant was collected. To further precipitate additional soluble compounds, the supernatant was mixed again with 96 % ethanol at a volume ratio of 50 %. The process of ethanol precipitation was repeated a total of three times, with each round followed by centrifugation to separate the precipitate from the supernatant.

To minimize interference caused by sodium ions, silver nitrate was added to the supernatant until it reached a concentration of 50 mM. This step was undertaken to reduce the presence of sodium ions, which can affect the accuracy of the measurement. Following this, the mixture underwent centrifugation at 20,000 g for 2 min to remove any remaining sediments. The resulting supernatant, now free from sediment and with reduced sodium ion content, was utilized for identifying thiabendazole. For the identification process, 10 μl of the sample was dropped onto a substrate placed on a gold-coated slide. The sample-loaded substrate was dried under ambient conditions, and then measured by a Raman spectrometer (DXR2, ThermoFisher Scientific Inc), allowing for the analysis of the vibrational spectra and subsequent identification of the presence of thiabendazole (Wang, Li, Lin, Chen, Zhang, & Yang, 2021). On each substrate with samples, 20 points were randomly selected to acquire spectra, which were then averaged to generate a representative spectrum of the sample. The Raman spectrum was scanned across a range of wavenumbers from 500 to 2000 cm^{-1}. This range encompasses the desired vibrational modes and provides detailed information about the molecular structure and composition of the analytes. During the Raman measurements, the power of 785-nm laser source was set at 20 mW. This power level ensured optimal excitation of the analytes without causing any significant degradation or alteration of the samples (Asgari et al., 2020).

2.6. Data analysis

The analysis of data and processing of spectroscopic measurements involved the use of specific software tools. To assess the significance of differences between groups, the Duncan's Multiple Range Test (DMRT) was performed using the SPSS software (IBM SPSS Statistics, version 19), with a confidence coefficient of 0.05 % ($p < 0.05$). The results were reported as ± standard deviations, providing an indication of the data's variability. The limit of detection (LOD) and limit of quantification (LOQ) for our analysis were determined using standard procedures. The LOD, defined as the lowest analyte concentration reliably distinguishable from a blank sample, was calculated as three times the standard deviation of the blank signal divided by the slope of the calibration curve. The LOQ, representing the lowest analyte concentration quantifiable with acceptable precision, was determined as ten times the standard deviation of the blank signal divided by the slope of the calibration curve. These calculations were performed based on multiple replicates of blank samples and calibration standards, ensuring the robustness and accuracy of our analytical method. For the collection and analysis of Raman and FTIR data, the OMNIC software (ThermoFisher Scientific Inc.) was utilized. This software facilitated the acquisition of spectral data from the samples, allowing for initial processing and visualization of the spectra. To enhance the quality and resolution of the spectra, as well as to remove noise and smooth the peaks, the Delight software (Delight, D-squared Development Inc., LaGrande, OR, USA) was employed to obtain reliable and high-quality results for subsequent analysis and interpretation.

3. Results and discussion

3.1. Scaffold characterization

The optimization of the electrospinning process for producing PAN nanofibers focused on varying flow rate variables, distance to the collector, and applied voltage. The primary objective of this optimization was to achieve uniform, bead-free nanofibers. It is important to note that Triton X-100 served as a surfactant during the electrospinning process.

Firstly, flow rate variables play a crucial role in the electrospinning process as they determine the rate at which the polymer solution is ejected from the spinneret. Higher flow rates generally lead to faster polymer solution deposition, resulting in thicker fibers with an increased likelihood of bead formation. Conversely, lower flow rates may lead to thinner fibers, but with slower deposition rates. To optimize the production process and achieve uniform and bead-free nanofibers, different ranges of flow rate variables were investigated. This involved systematically varying the flow rate to identify the optimal range that promotes the formation of uniform nanofibers without beads (Hajikhani et al., 2022).

Another critical parameter for optimization is the distance between

the spinneret and the collector. This distance affects the stretching and solidification of the ejected polymer solution, which directly influences the morphology of nanofibers. A shorter distance promotes rapid solvent evaporation, resulting in thicker fibers and a higher chance of bead formation. Conversely, a longer distance allows for more stretching and thinning of the polymer solution but may lead to erratic fiber deposition and reduced production rates. By exploring different distances to the collector, the optimal range can be determined to achieve uniform and bead-free nanofibers (Hajikhani et al., 2022).

The applied voltage is also a key factor in the electrospinning process as it creates an electric field that facilitates the elongation and stretching of the polymer solution into nanofibers. Higher voltages generally result in stronger electric fields, leading to faster solvent evaporation and increased stretching of the polymer solution. However, excessively high voltages can cause instability in the jet, resulting in bead formation or fiber breakage. Conversely, lower voltages may lead to insufficient stretching and thinning of the polymer solution, resulting in thicker fibers. The optimization process involves exploring different voltage ranges to find the optimal value that promotes the formation of uniform and bead-free nanofibers (Hajikhani et al., 2022).

In the optimization process, Triton X-100 was utilized as a surfactant. It is commonly employed in electrospinning to enhance the viscosity and surface tension of the polymer solution. Its incorporation can improve the electrospinning process by reducing bead formation and promoting a uniform fiber morphology (Aykut, Pourdeyhimi, & Khan, 2013).

Throughout the optimization process, different ranges of flow rates, distances to the collector, and applied voltages were explored. Flow rates ranged from 0.5 to 2 ml/h, distances to the collector spanned from 10 to 30 cm, and voltages varied between 10 and 20 kV. After a series of experiments, the ideal conditions were determined to be a flow rate of 1 ml/h, a distance of 20 cm from the collector, and a voltage of 12 kV. Under these optimal conditions, a stable Taylor's cone formed, and the resulting nanofibers exhibited a uniform structure without any bead formation. This signifies the successful achievement of the optimization goal, demonstrating that the selected parameter values contribute to the production of uniform and bead-free nanofibers.

3.2. TEM coupled with EDS

The core–shell structure of a gold-silver sample was investigated

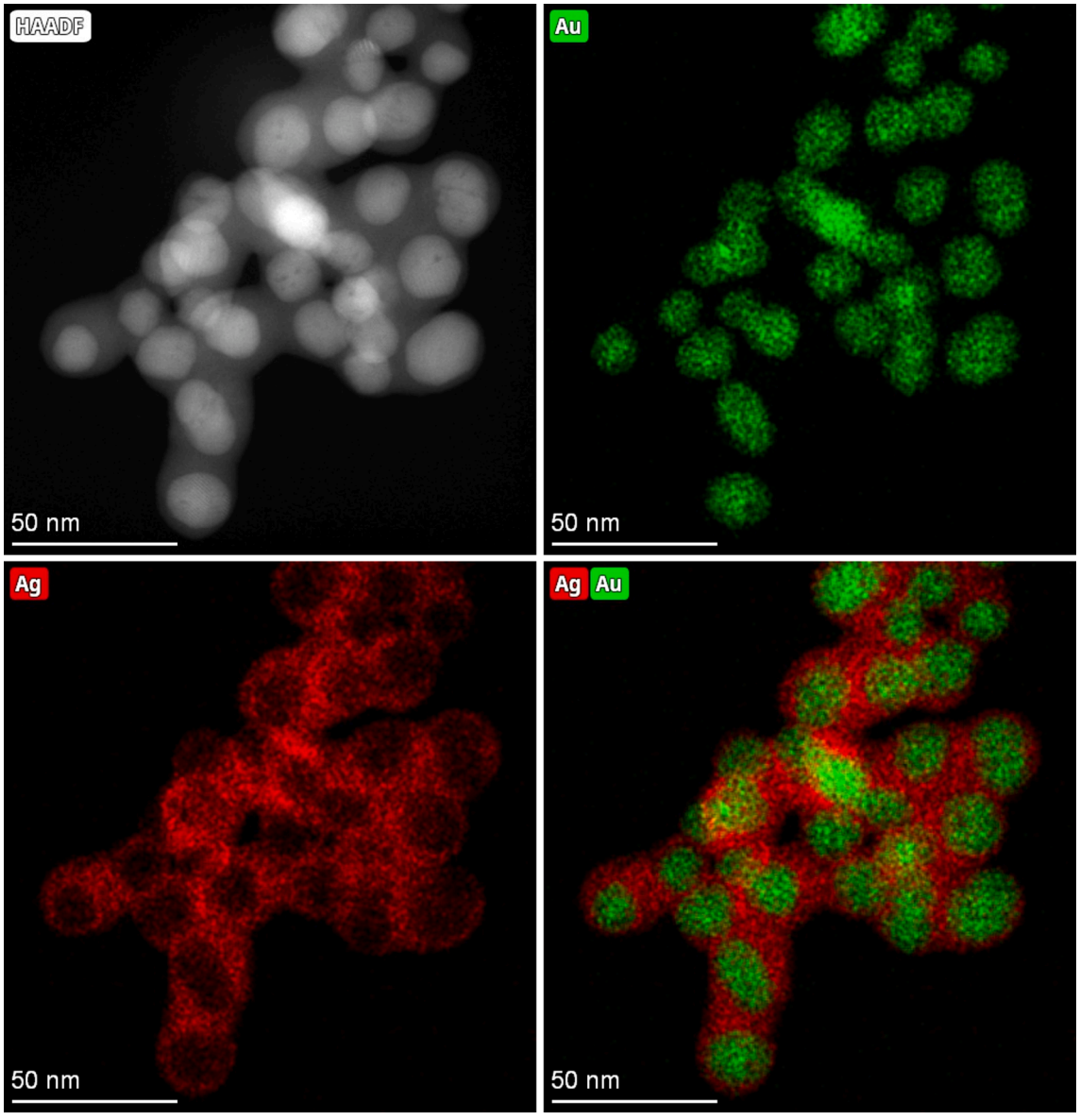

Fig. 2. The core–shell nanoparticles revealed through a transmission electron microscopy technique coupled with energy-dispersive X-ray spectroscopy.

using TEM-EDS analysis. The average particle diameter of the core–shell nanoparticles was determined to be 23.58 ± 3.87 nm. TEM imaging provided high-resolution images, revealing the distinct core and shell regions within each particle. The gold core appeared as a bright contrast, surrounded by a dark silver shell, confirming the successful synthesis of the core–shell architecture (Fig. 2). EDS analysis further confirmed the elemental composition, with characteristic X-ray signals observed for both gold and silver. The precise characterization of the core–shell morphology and elemental distribution using TEM-EDS analysis contributes to the understanding of the structural properties and potential applications of these nanoparticles in various fields, such as catalysis, nanomedicine, and sensing.

TEM-EDS analysis was conducted on the electrospun nanofiber sample to investigate its structural characteristics, particularly in terms of surface modification with core–shell nanoparticles. The mean diameter of the nanofibers was calculated to be 507.61 ± 6.42 nm, and the diameter distribution fell within an acceptable range. The surface morphology of the nanofibers exhibited a smooth texture, indicating a well-controlled electrospinning process (Fig. 3A). Detailed TEM images were obtained to visualize the surface modification of the nanofibers and the subsequent coating with core–shell nanoparticles. EDS scanning provided conclusive evidence of the successful coverage of the nanofiber surface with the core–shell nanoparticles. Furthermore, it was observed that the surface morphology of the nanofibers underwent a significant transformation, becoming completely rough after the surface modification (Fig. 3B & 3C). This change in surface morphology suggests the effective incorporation of the core–shell nanoparticles onto the nanofiber surface. The TEM-EDS analysis provides crucial insights into the

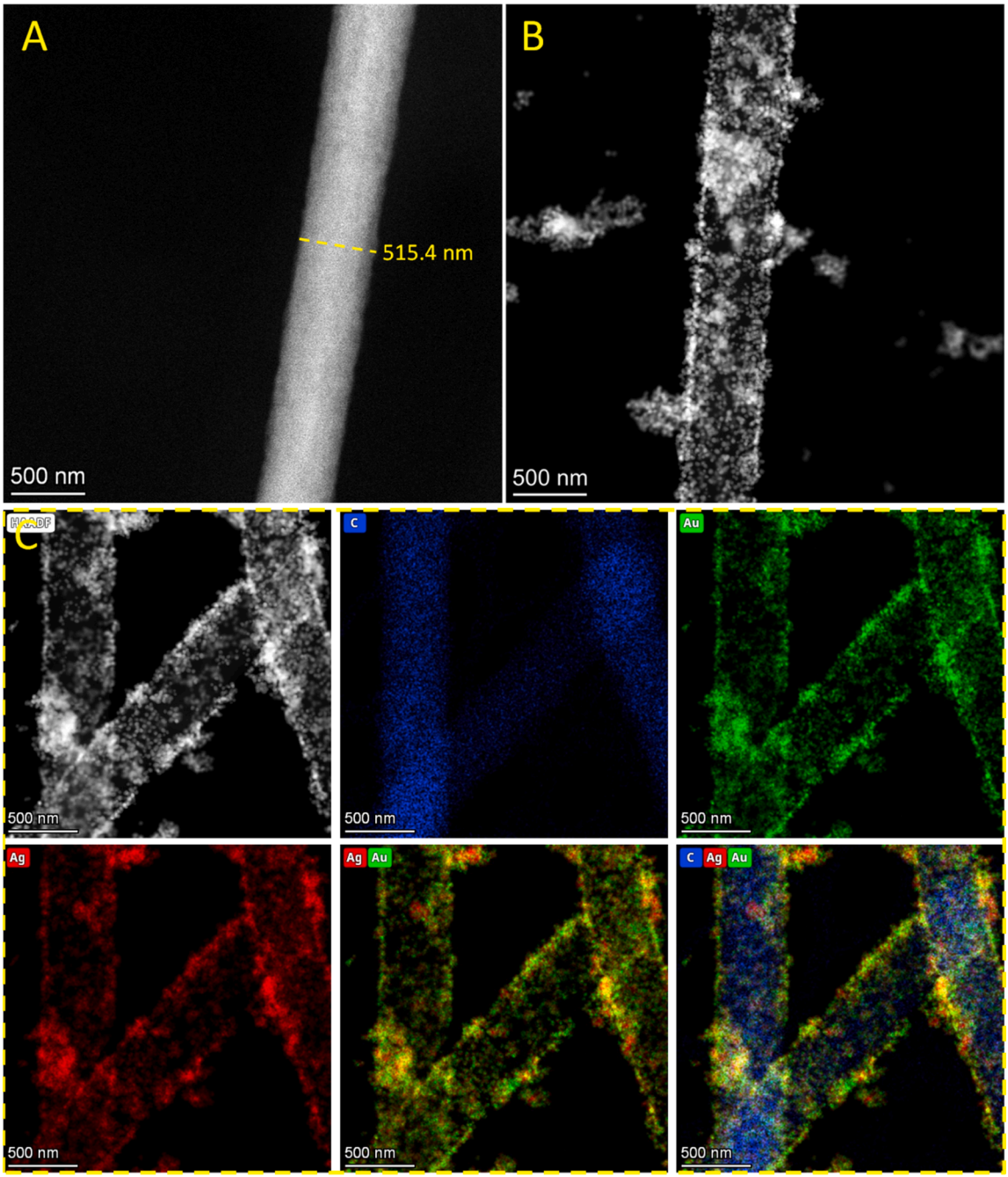

Fig. 3. The transmission electron microscopy (TEM) images capturing the morphology of PAN nanofibers both prior to and after undergoing surface modification (A and B, respectively); the TEM-EDS images illustrating the PAN nanofibers (C).

structural and morphological characteristics of the electrospun nanofiber sample, specifically in relation to its surface modification and the subsequent coating with core–shell nanoparticles. These findings help advance the understanding of nanofiber functionalization for various applications, such as SERS substrates (Chen, Gupta, & Chattopadhyay, 2021).

3.3. Chemical functionalization

To enhance the capabilities of electrospun PAN nanofibers for specific applications, a surface modification technique was employed. PAN polymer possesses a nitrile functional group (−C≡N) that can be utilized immobilizing EDTA. However, prior to immobilizing EDTA, it was necessary to introduce the NH_2 (amino) functional group onto the nanofiber surface (Chaúque et al., 2016). To achieve this, an ethylenediamine solution was utilized as a crosslinker. Ethylenediamine plays a dual role in this process. Firstly, it forms a bond with the nitrile functional group of PAN nanofibers, resulting in an enrichment of NH_2 groups on the nanofiber surface. Secondly, EDTA reacts with the EDC reagent, facilitating the chemical interaction between the carboxyl groups of EDTA and the NH_2 groups of the nanofibers treated with ethylenediamine (Chaúque et al., 2017).

The modified nanofibers, treated with ethylenediamine and possessing NH_2 groups, were then immersed in an EDTA solution. At this step, EDC acted as a chemical mediator, promoting chemical interaction between the carboxyl groups of EDTA and the NH_2 groups on the nanofiber surface. This resulted in the immobilization of EDTA onto the nanofibers, enabling them to exhibit chelating properties towards heavy metals (Chaúque et al., 2017; Chaúque et al., 2019). To further enhance the functionality of the modified nanofibers, they were incubated in a nanoparticle solution to facilitate the coating of core–shell nanoparticles. The nanoparticles used in this study were specifically chosen based on their compatibility with the immobilized EDTA. EDTA, with its ability to chelate heavy metals, effectively absorbed the core–shell nanoparticles, allowing them to coat the surface of PAN nanofibers (Fig. 4). The resulting composite scaffold exhibited an enhanced capacity for heavy metal removal.

The final scaffold, modified with EDTA and coated with core–shell nanoparticles, was employed as a substrate for the detection of thiabendazole using the SERS method. Fig. 4 displays the images illustrating the scaffold treatment and functionalization. This combination of surface functionalization and nanoparticle coating provided an effective platform for sensitive and selective detection of thiabendazole, demonstrating the potential of the modified nanofibers in environmental monitoring and analytical applications. To assess the performance of the designed substrate for thiabendazole detection, a series of experiments were conducted using different concentrations of thiabendazole solutions. The concentration range considered for the evaluation ranged from 10 ppb to 5 ppm.

The resulting Raman spectra obtained from the measurements are depicted in Fig. 5A. To investigate the relationship between the concentration of the analyte (thiabendazole) and the intensity of Raman signals, six peaks along the spectrum were selected and subjected to further analysis (Nie, Dong, Xiao, Lin, He, & Qu, 2018), revealing that there is a linear relationship between the concentration of thiabendazole and the corresponding intensity of the peaks. The determination coefficient (R^2) was calculated for each peak, indicating the goodness of fit for the linear relationship. Peaks corresponding to wavenumbers 771, 883, 981, and 1001 cm^{-1} exhibited high R^2 values, all exceeding 99 %. However, the peaks corresponding to wavenumbers 1592 and 1626 cm^{-1} showed R^2 values of 96 % and 93 %, respectively. The peak at the wavenumber 1001 cm^{-1} was chosen for determining the LOD and LOQ due to its excellent R^2 value. The concentration range of 10 to 1000 ppb was utilized for the calculations as it demonstrated a more linear response. The LOD and LOQ were determined as 47.4 and 125.5 ppb, respectively, with an R^2 value of 99.91 %.

Based on these findings, it can be concluded that the designed substrate exhibits a high capability to amplify the Raman signals and demonstrates excellent potential for application in quantitative detection systems. The linear relationship observed between analyte concentration and intensity, along with the high R^2 values obtained for most peaks, validates the effectiveness of the substrate for sensitive detection and quantification of thiabendazole.

3.4. FTIR

FTIR analysis of PAN polymer involves studying specific peaks related to its molecular structure (Fig. 5B). The nitrile stretching peak at 2240–2250 cm^{-1} corresponds to the carbon–nitrogen triple bond (C≡N) present in acrylonitrile units, providing information on the polymerization degree and acrylonitrile concentration. The C—H stretching peaks at 2920–2980 cm^{-1} represent methylene groups (–CH2-) and offer insights into chain conformation and the presence of side groups or impurities. PAN exhibits a characteristic C≡N bending peak at 1610–1620 cm^{-1}, which reveals information about chain orientation and crystallinity (Data was not shown). The C═O stretching peaks at 1700–1730 cm^{-1} indicate carbonyl groups resulting from oxidation or degradation, reflecting the sample's extent of degradation. Finally, the C—C stretching peaks at 1440–1470 cm^{-1} provide information on polymer chain structure, branching, or cross-linking (Zhang et al., 2010).

The analysis of FTIR peaks related to EDTA reveals important information about its molecular structure and functional groups. The carboxylic acid stretching peak at 1710–1720 cm^{-1} indicates the presence and degree of carboxylic acid groups in EDTA. The carboxylate stretching peak at 1400–1600 cm^{-1} provides information about the presence and concentration of carboxylate groups resulting from the ionization of carboxylic acid groups. The C—N stretching peak at 1050–1100 cm^{-1} reflects the concentration and bonding environment of the amine groups. Analyzing these FTIR peaks helps in understanding the molecular characteristics and quality of EDTA samples for various applications (Chaúque et al., 2017).

The FTIR spectrum analysis of a PAN polymer sample treated with ethylenediamine reveals important information about the molecular

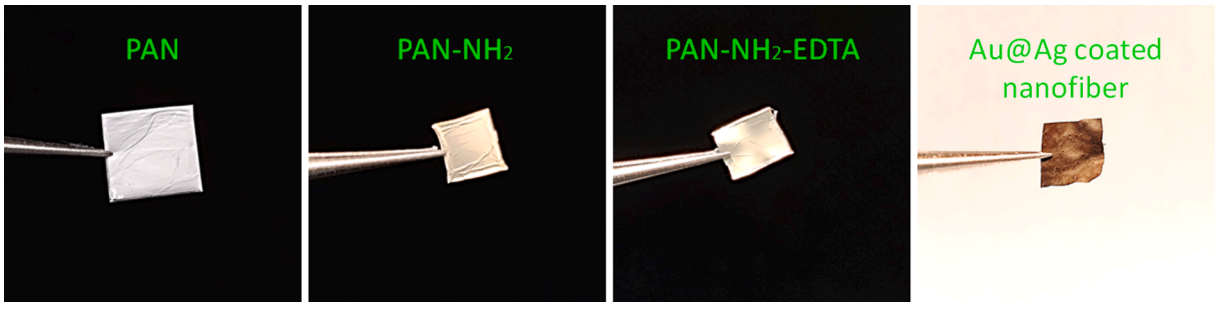

Fig. 4. Different stages of functionalization, immobilization, and coating of the substrate.

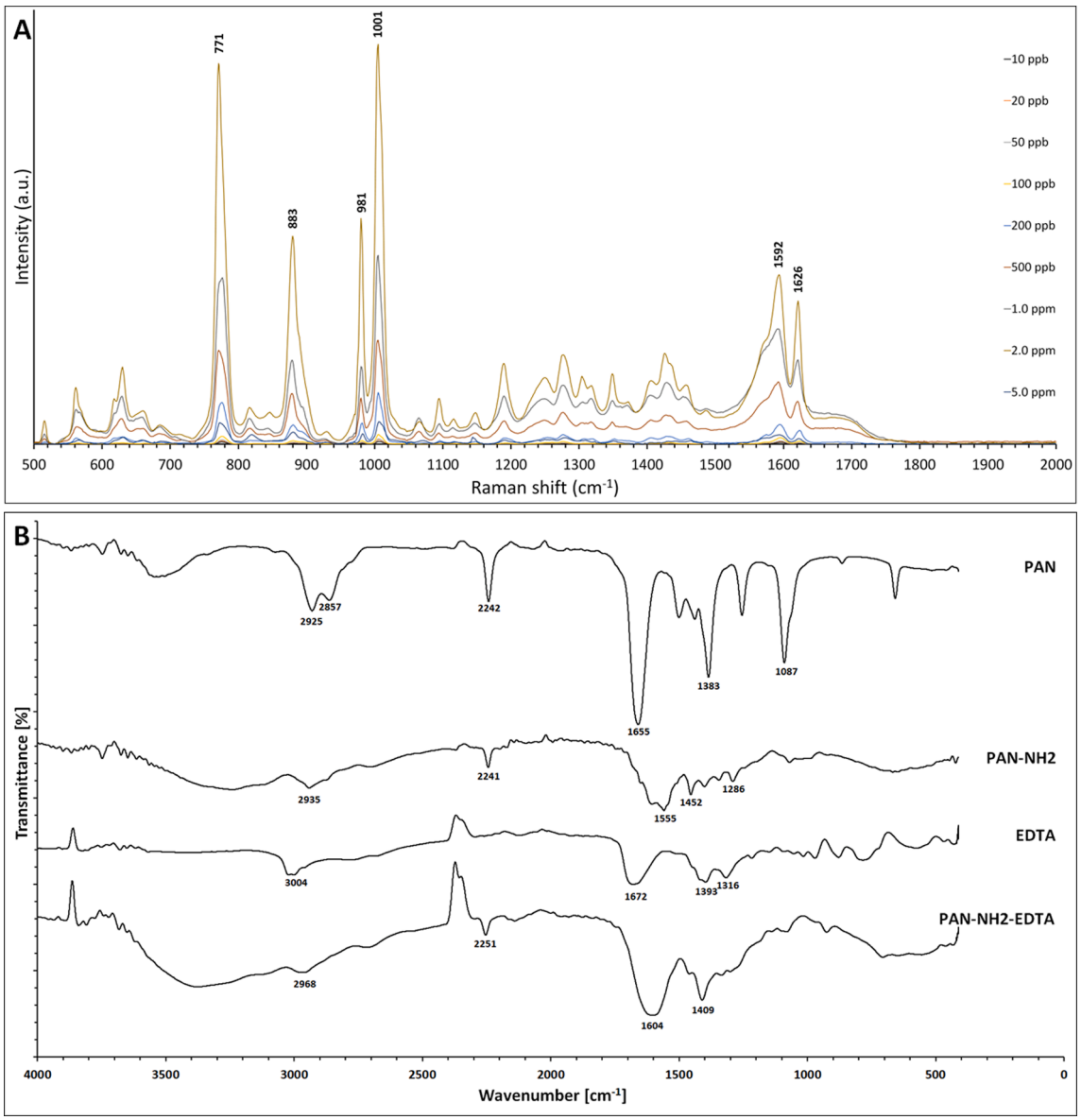

Fig. 5. The spectra of different concentrations of thiabendazole (A) and different FTIR spectra related to different stages of SERS substrate design (B).

interactions and modifications occurring in the polymer. The presence of ethylenediamine can be identified through the characteristic peaks observed in the spectrum. The amine stretching peak around 3100–3500 cm^{-1} indicates the presence and concentration of amine groups in ethylenediamine (Li et al., 2017). The amine bending peaks around 1450–1650 cm^{-1} provide insights into the molecular conformation and interactions of ethylenediamine. Additionally, the C—C stretching peaks around 1400–1500 cm^{-1} reflect the molecular connectivity and bonding in ethylenediamine. By analyzing the changes in the intensity and shape of these peaks, valuable insights can be gained into the interaction between ethylenediamine and the PAN polymer, which can have implications for polymer functionality, structure, and potential applications (Tsirul'nikova & Volkov, 2018).

The decrease in the intensity of the peak at 2242 cm^{-1} in the PAN polymer sample treated with ethylenediamine compared to the untreated PAN sample suggests a modification or interaction involving the nitrile group (C≡N) in PAN. In the untreated PAN sample, this peak corresponds to the nitrile stretching vibration, indicating the presence of acrylonitrile monomer units in the polymer. However, the decrease in intensity suggests that the interaction between ethylenediamine and PAN could lead to a change in the concentration or bonding environment of the nitrile groups. It is possible that ethylenediamine may be involved in a reaction or coordination with the nitrile groups, causing a reduction in the intensity of the peak (Qiao et al., 2019).

The FTIR spectrum analysis of a PAN-NH_2 sample treated with EDTA offers valuable insights into the molecular interactions and modifications occurring in the polymer. Several peaks related to EDTA were observed in the spectrum that provide information about the presence and changes in functional groups. The carboxylic acid stretching peak around 1700 cm^{-1} indicates the presence and degree of carboxylic acid groups from EDTA in the PAN-NH_2-EDTA sample. The amine stretching peak around 3200–3500 cm^{-1} reveals the presence and concentration of amine groups in EDTA, which can be seen in the PAN-NH2-EDTA sample. The carboxylate stretching peak around 1400 cm^{-1} corresponds to the stretching vibration of the C—O bond in carboxylate groups formed through the ionization of carboxylic acid groups in EDTA (Lanigan & Pidsosny, 2007). By analyzing these peaks, a comprehensive understanding of the interactions between ethylenediamine, EDTA, and the PAN polymer can be obtained.

The decrease in intensity and the shift to a higher wavenumber for the peak at 2242 cm^{-1} suggest that the interaction with EDTA leads to a change in the concentration or bonding environment of the nitrile

groups. The shift to a higher wavenumber indicates a stronger bond or a change in the bond strength between the carbon and nitrogen atoms. Additionally, the decrease in intensity suggests a potential reaction or coordination between EDTA and the PAN-NH_2 sample, causing a reduction in the concentration of these groups or a modification of their bonding environment. This change in intensity and shift in wavenumber highlights the importance of FTIR spectrum analysis in studying the effects of treatments or interactions on the PAN polymer's structure and properties (Mantripragada, Deng, & Zhang, 2021).

3.5. Detection of thiabendazole in soy-based food samples

The identification of thiabendazole in soy-based food samples, such as soy milk and soy sauce, is of significant importance for several reasons. Firstly, thiabendazole is a commonly used fungicide in agriculture, and its presence in food samples raises concerns about potential consumer exposure to this chemical compound. Understanding the levels and frequency of thiabendazole contamination in soy-based products allows for a comprehensive assessment of consumer safety and potential health risks associated with its consumption (Sun, He, Yang, Li, Zhao, & Li, 2017). Additionally, soy-based foods are widely consumed globally, particularly by individuals with dietary restrictions or preferences. Hence, monitoring thiabendazole residues in these products is crucial for ensuring the quality, safety, and compliance of the food supply chain. Furthermore, the identification of thiabendazole in soy-based food samples can contribute to establishing regulatory standards and guidelines, enabling the implementation of appropriate control measures to minimize thiabendazole contamination and protect public health. Ultimately, this research aids in enhancing consumer confidence and promoting the production and consumption of safe and contaminant-free soy-based food products.

The soy sauce sample was analyzed for the detection of thiabendazole, using a concentration range of 100 to 1000 ppb. The peak corresponding to 1592 cm^{-1}, associated with C═N stretching modes, was utilized to assess linearity (Lin et al., 2018). It was observed that as the concentration increased from 1 ppm and above, the intensity exhibited a non-linear increase. The LOQ was determined to be 240.59 ppb, while the LOD was calculated to be 79.4 ppb. Interestingly, a linear relationship between intensity and concentration was observed within the range below 1 ppm, with an R^2 value of 99.42 %. However, the obtained spectra exhibited significant noise, possibly attributed to the high percentage of sodium ions present in soy sauce. Fig. 6A illustrates the resulting spectra obtained during the analysis. These findings provide valuable insights into the detection and quantification of thiabendazole in soy sauce samples, while acknowledging the challenges posed by the background noise arising from the sodium content.

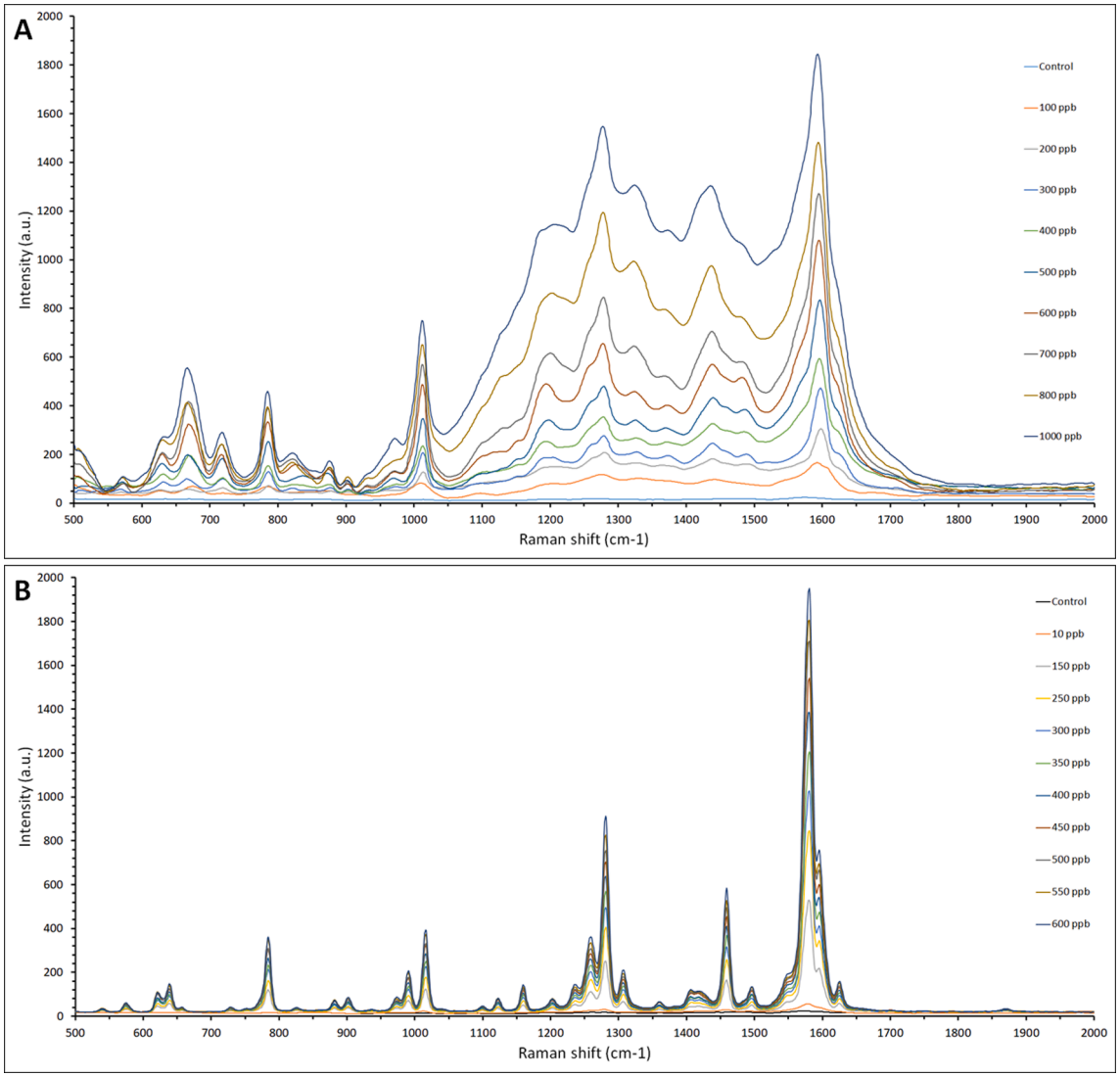

Fig. 6. Different Raman spectra related to different concentrations of thiabendazole in soy sauce samples (A) and in soymilk samples (B).

In the detection of thiabendazole in the soy milk sample, a concentration range of 10 to 600 ppb was employed because it showed a more linear correlation in this concentration range. Similar to the soy sauce sample, the peak corresponding to 1580 cm^{-1}, associated with C═N stretching modes, was utilized to assess linearity. Concentrations exceeding 1 ppm displayed exponential behavior in intensity. The LOQ for thiabendazole in soy milk was determined as 69.9 ppb, while the LOD was calculated to be 23.1 ppb, indicating the sensitivity of the method. The coefficient of determination within this concentration range was found to be 99.75 %, demonstrating a strong correlation between concentration and intensity. Notably, the peaks obtained from the soy milk sample appeared smoother with less noise compared to those observed in the soy sauce sample. Fig. 6B illustrates the resulting spectra obtained during the analysis, highlighting the distinct characteristics of the soy milk sample. These findings provide valuable insights into the detection and quantification of thiabendazole in soy milk samples, emphasizing the improved peak quality and sensitivity of the analysis in this food matrix.

The detection of thiabendazole in food samples has yielded varied results across different studies. The LOD for thiabendazole in tea samples was recorded as 100 ppb (Ding et al., 2019), while apple juice, peach juice, and soy milk samples exhibited LODs of 32 ppb (Z. Chen et al., 2022), 34 ppb (Z. Chen et al., 2022), and 39 ppb (Hussain, Pu, & Sun, 2020), respectively. When compared to the findings of other studies, the results obtained in this study hold significant value. An important aspect of the new technique employed in this study was the achievement of uniform intensity at different points of the substrate. This uniformity allowed for the collection of data with higher accuracy and precision. This improvement in intensity uniformity contributes to the reliability and validity of the results obtained, further emphasizing the importance of the technique utilized in this study. Overall, the findings of this study provide valuable insights into the detection of thiabendazole in various food samples and highlight the advancements in analytical techniques, ensuring more accurate and reliable data acquisition.

4. Conclusion

In conclusion, the detection of thiabendazole in soy-based food samples is of great importance for ensuring consumer safety, regulatory compliance, and the overall quality of the food supply chain. Thiabendazole, a commonly used fungicide in agriculture, can potentially pose health risks if present in food products. This research aimed to assess the levels and frequency of thiabendazole contamination in soy-based foods, specifically soy milk and soy sauce. The study utilized a detection method based on analyzing the Raman spectra of the samples. The C═N stretching modes at 1592 and 1580 cm^{-1} were used to assess linearity and quantify thiabendazole concentrations. The results demonstrated a linear relationship between intensity and concentration within the range of 100 to 1000 ppb for soy sauce sample and 10 to 600 ppb for soy milk sample, with high coefficient of determination values (99.75 % and 99.42 % respectively). The LOQ were determined to be 69.9 and 240.59 ppb for soy milk and soy sauce samples respectively, indicating the sensitivity of the method, while the LOD were 23.1 ppb for soy milk and 79.4 ppb for soy sauce. Despite challenges posed by background noise, particularly from sodium ions in soy sauce, the method proved effective in detecting and quantifying thiabendazole in both samples. The findings contribute to the understanding of thiabendazole contamination in soy-based foods and provide valuable insights for establishing regulatory standards and guidelines. Moreover, the study highlights the advancements in analytical techniques, such as Raman spectroscopy, that enable more accurate and reliable detection of thiabendazole in complex food matrices.

CRediT authorship contribution statement

Mehdi Hajikhani: Project administration, Conceptualization, Investigation, Data curation, Writing – original draft. **Seyedehalaleh Kousheh:** Data curation. **Yi Zhang:** Writing – review & editing. **Mengshi Lin:** Supervision, Funding acquisition, Writing – review & editing.

Declaration of Competing Interest

The authors declare that they have no known competing financial interests or personal relationships that could have appeared to influence the work reported in this paper.

Data availability

Data will be made available on request.

Acknowledgements

This research was financially supported by the USDA National Institute of Food and Agriculture (2019-67021-29859, 2020-67030-31336, 2023-67017-40165), the National Science Foundation (CBET-2103025), and the Robert T. Marshall Scholarship.

References

Asgari, S., Sun, L., Lin, J., Weng, Z., Wu, G., Zhang, Y., & Lin, M. (2020). Nanofibrillar cellulose/Au@Ag nanoparticle nanocomposite as a SERS substrate for detection of paraquat and thiram in lettuce. *Microchimica Acta, 187*(7), 390. https://doi.org/10.1007/s00604-020-04358-9

Aykut, Y., Pourdeyhimi, B., & Khan, S. A. (2013). Effects of surfactants on the microstructures of electrospun polyacrylonitrile nanofibers and their carbonized analogs. *Journal of Applied Polymer Science, 130*(5), 3726–3735. https://doi.org/10.1002/app.39637.

Bajwa, U., & Sandhu, K. S. (2014). Effect of handling and processing on pesticide residues in food- a review. *Journal of Food Science and Technology, 51*(2), 201–220. https://doi.org/10.1007/s13197-011-0499-5

Chamuah, N., Bhuyan, N., Das, P. P., Ojah, N., Choudhary, A. J., Medhi, T., & Nath, P. (2018). Gold-coated electrospun PVA nanofibers as SERS substrate for detection of pesticides. *Sensors and Actuators B: Chemical, 273*, 710–717. https://doi.org/10.1016/j.snb.2018.06.079.

Chaúque, E. F. C., Dlamini, L. N., Adelodun, A. A., Greyling, C. J., & Catherine Ngila, J. (2016). Modification of electrospun polyacrylonitrile nanofibers with EDTA for the removal of Cd and Cr ions from water effluents. *Applied Surface Science, 369*, 19–28. https://doi.org/10.1016/j.apsusc.2016.02.018.

Chaúque, E. F. C., Dlamini, L. N., Adelodun, A. A., Greyling, C. J., & Ngila, J. C. (2017). Electrospun polyacrylonitrile nanofibers functionalized with EDTA for adsorption of ionic dyes. *Physics and Chemistry of the Earth, Parts A/B/C, 100*, 201–211. https://doi.org/10.1016/j.pce.2016.10.008.

Chaúque, E. F. C., Ngila, J. C., Ray, S. C., & Ndlwana, L. (2019). Degradation of methyl orange on Fe/Ag nanoparticles immobilized on polyacrylonitrile nanofibers using EDTA chelating agents. *Journal of Environmental Management, 236*, 481–489. https://doi.org/10.1016/j.jenvman.2019.02.023.

Chen, B., Zhao, H., Chen, S., Long, F., Huang, B., Yang, B., & Pan, X. (2019). A magnetically recyclable chitosan composite adsorbent functionalized with EDTA for simultaneous capture of anionic dye and heavy metals in complex wastewater. *Chemical Engineering Journal, 356*, 69–80. https://doi.org/10.1016/j.cej.2018.08.222.

Chen, H., Lin, J., Zhang, N., Chen, L., Zhong, S., Wang, Y., … Ling, Q. (2018). Preparation of MgAl-EDTA-LDH based electrospun nanofiber membrane and its adsorption properties of copper(II) from wastewater. *Journal of Hazardous Materials, 345*, 1–9. https://doi.org/10.1016/j.jhazmat.2017.11.002.

Chen, M., Zhang, J., Zhu, X., Liu, Z., Huang, J., Jiang, X., … Dong, Y. (2022). Hybridizing Silver Nanoparticles in Hydrogel for High-Performance Flexible SERS Chips. *ACS Applied Materials & Interfaces, 14*(22), 26216–26224. https://doi.org/10.1021/acsami.2c04087

Chen, X., Lin, M., Sun, L., Xu, T., Lai, K., Huang, M., & Lin, H. (2019). Detection and quantification of carbendazim in Oolong tea by surface-enhanced Raman spectroscopy and gold nanoparticle substrates. *Food Chemistry, 293*, 271–277. https://doi.org/10.1016/j.foodchem.2019.04.085.

Chen, Z.-Y., Gupta, A., & Chattopadhyay, S. (2021). Detection of mercury in spiked cosmetics by surface enhanced Raman spectroscopy using silver shelled iron oxide

nanoparticles. *Sensors and Actuators B: Chemical, 337*, Article 129788. https://doi.org/10.1016/j.snb.2021.129788.
Chen, Z., Sun, Y., Shi, J., Zhang, W., Zhang, X., Huang, X., … Wei, R. (2022). Facile synthesis of Au@Ag core–shell nanorod with bimetallic synergistic effect for SERS detection of thiabendazole in fruit juice. *Food Chemistry, 370*, Article 131276. https://doi.org/10.1016/j.foodchem.2021.131276.
Choi, S.-I., Han, X., Lee, S.-J., Men, X., Oh, G., Lee, D.-S., & Lee, O.-H. (2022). Validation of an Analytical Method for the Determination of Thiabendazole in Various Food Matrices. *Separations, 9*(6), 135. https://www.mdpi.com/2297-8739/9/6/135.
Cong, S., Yuan, Y., Chen, Z., Hou, J., Yang, M., Su, Y., … Zhao, Z. (2015). Noble metal-comparable SERS enhancement from semiconducting metal oxides by making oxygen vacancies. *Nature Communications, 6*(1), 7800. https://doi.org/10.1038/ncomms8800
Deng, S., Liu, X., Liao, J., Lin, H., & Liu, F. (2019). PEI modified multiwalled carbon nanotube as a novel additive in PAN nanofiber membrane for enhanced removal of heavy metal ions. *Chemical Engineering Journal, 375*, Article 122086. https://doi.org/10.1016/j.cej.2019.122086.
Ding, Q., Kang, Z., He, X., Wang, M., Lin, M., Lin, H., & Yang, D.-P. (2019). Eggshell membrane-templated gold nanoparticles as a flexible SERS substrate for detection of thiabendazole. *Microchimica Acta, 186*(7), 453. https://doi.org/10.1007/s00604-019-3543-1
Flores Kim, J., McCleary, N., Nwaru, B. I., Stoddart, A., & Sheikh, A. (2018). Diagnostic accuracy, risk assessment, and cost-effectiveness of component-resolved diagnostics for food allergy: A systematic review. *Allergy, 73*(8), 1609–1621. https://doi.org/10.1111/all.13399.
Hajikhani, M., & Lin, M. (2022). A review on designing nanofibers with high porous and rough surface via electrospinning technology for rapid detection of food quality and safety attributes. *Trends in Food Science & Technology, 128*, 118–128. https://doi.org/10.1016/j.tifs.2022.08.003.
Hassan, M. M., Xu, Y., Zareef, M., Li, H., Rong, Y., & Chen, Q. (2021). Recent advances of nanomaterial-based optical sensor for the detection of benzimidazole fungicides in food: A review. *Critical Reviews in Food Science and Nutrition, 1–22*. https://doi.org/10.1080/10408398.2021.1980765
Hou, D., O'Connor, D., Igalavithana, A. D., Alessi, D. S., Luo, J., Tsang, D. C. W., … Ok, Y. S. (2020). Metal contamination and bioremediation of agricultural soils for food safety and sustainability. *Nature Reviews Earth & Environment, 1*(7), 366–381. https://doi.org/10.1038/s43017-020-0061-y
Hussain, A., Pu, H., & Sun, D.-W. (2020). SERS detection of sodium thiocyanate and benzoic acid preservatives in liquid milk using cysteamine functionalized core-shelled nanoparticles. *Spectrochimica Acta Part A: Molecular and Biomolecular Spectroscopy, 229*, Article 117994. https://doi.org/10.1016/j.saa.2019.117994.
Jallow, A., Xie, H., Tang, X., Qi, Z., & Li, P. (2021). Worldwide aflatoxin contamination of agricultural products and foods: From occurrence to control. *Comprehensive Reviews in Food Science and Food Safety, 20*(3), 2332–2381. https://doi.org/10.1111/1541-4337.12734.
Lanigan, K. C., & Pidsosny, K. (2007). Reflectance FTIR spectroscopic analysis of metal complexation to EDTA and EDDS. *Vibrational Spectroscopy, 45*(1), 2–9. https://doi.org/10.1016/j.vibspec.2007.03.003.
Lee, H., Nishino, M., Sohn, D., Lee, J. S., & Kim, I. S. (2018). Control of the morphology of cellulose acetate nanofibers via electrospinning. *Cellulose, 25*(5), 2829–2837. https://doi.org/10.1007/s10570-018-1744-0
Lee, H., & Yoon, Y. (2021). Etiological Agents Implicated in Foodborne Illness World Wide. *Food Sci Anim Resour, 41*(1), 1–7. https://doi.org/10.5851/kosfa.2020.e75
Li, D., Gu, Y., Feng, Y., Xu, X., Wang, M., & Liu, Y. (2020). Synthesis of silver nanoplates on electrospun fibers via tollens reaction for SERS sensing of pesticide residues. *Microchimica Acta, 187*(10), 560. https://doi.org/10.1007/s00604-020-04514-1
Li, P., Teng, Y., Nie, Y., & Liu, W. (2018). SERS Detection of Insecticide Amitraz Residue in Milk Based on Au@Ag Core-Shell Nanoparticles. *Food Analytical Methods, 11*(1), 69–76. https://doi.org/10.1007/s12161-017-0966-3
Li, Z., Zabihi, O., Wang, J., Li, Q., Wang, J., Lei, W., & Naebe, M. (2017). Hydrophilic PAN based carbon nanofibres with improved graphitic structure and enhanced mechanical performance using ethylenediamine functionalized graphene. *RSC Advances, 7*(5), 2621–2628. https://doi.org/10.1039/C6RA24719A
Liao, Y., Loh, C.-H., Tian, M., Wang, R., & Fane, A. G. (2018). Progress in electrospun polymeric nanofibrous membranes for water treatment: Fabrication, modification and applications. *Progress in Polymer Science, 77*, 69–94. https://doi.org/10.1016/j.progpolymsci.2017.10.003.
Lin, L., Dong, T., Nie, P., Qu, F., He, Y., Chu, B., & Xiao, S. (2018). Rapid Determination of Thiabendazole Pesticides in Rape by Surface Enhanced Raman Spectroscopy. *Sensors, 18*.
Lin, Z., & He, L. (2019). Recent advance in SERS techniques for food safety and quality analysis: A brief review. *Current Opinion in Food Science, 28*, 82–87. https://doi.org/10.1016/j.cofs.2019.10.001.
Liu, Y., Galani Yamdeu, J. H., Gong, Y. Y., & Orfila, C. (2020). A review of postharvest approaches to reduce fungal and mycotoxin contamination of foods. *Comprehensive Reviews in Food Science and Food Safety, 19*(4), 1521–1560. https://doi.org/10.1111/1541-4337.12562.
Logan, N., Haughey, S. A., Liu, L., Burns, D. T., Quinn, B., Cao, C., & Elliott, C. T. (2022). Handheld SERS coupled with QuEChERs for the sensitive analysis of multiple pesticides in basmati rice. *NPJ Science of Food, 6*(1), 3. https://doi.org/10.1038/s41538-021-00117-z
Mantripragada, S., Deng, D., & Zhang, L. (2021). Remediation of GenX from water by amidoxime surface-functionalized electrospun polyacrylonitrile nanofibrous adsorbent. *Chemosphere, 283*, Article 131235. https://doi.org/10.1016/j.chemosphere.2021.131235.
Nie, P., Dong, T., Xiao, S., Lin, L., He, Y., & Qu, F. (2018). Quantitative Determination of Thiabendazole in Soil Extracts by Surface-Enhanced Raman Spectroscopy. *Molecules (Basel, Switzerland)* (Vol. 23).
Ons, L., Bylemans, D., Thevissen, K., & Cammue, B. P. A. (2020). Combining biocontrol agents with chemical fungicides for integrated plant fungal disease control. *Microorganisms, 8*(12). https://doi.org/10.3390/microorganisms8121930
Petersen, M., Yu, Z., & Lu, X. (2021). Application of Raman spectroscopic methods in food safety: A review. *Biosensors, 11*.
Qiao, M., Kong, H., Ding, X., Hu, Z., Zhang, L., Cao, Y., & Yu, M. (2019). Study on the changes of structures and properties of PAN fibers during the cyclic reaction in supercritical carbon dioxide. *Polymers (Basel), 11*(3). https://doi.org/10.3390/polym11030402
Qin, P., Wang, T., & Luo, Y. (2022). A review on plant-based proteins from soybean: Health benefits and soy product development. *Journal of Agriculture and Food Research, 7*, Article 100265. https://doi.org/10.1016/j.jafr.2021.100265.
Shao, F., Cao, J., Ying, Y., Liu, Y., Wang, D., Guo, X., … Yang, H. (2020). Preparation of Hydrophobic film by electrospinning for rapid SERS detection of trace triazophos. *Sensors, 20*.
Singh, N., Prakash, J., Misra, M., Sharma, A., & Gupta, R. K. (2017). Dual functional Ta-doped electrospun TiO2 nanofibers with enhanced photocatalysis and SERS detection for organic compounds. *ACS Applied Materials & Interfaces, 9*(34), 28495–28507. https://doi.org/10.1021/acsami.7b07571
Sridhar, A., Ponnuchamy, M., Kapoor, A., & Prabhakar, S. (2022). Valorization of food waste as adsorbents for toxic dye removal from contaminated waters: A review. *Journal of Hazardous Materials, 424*, Article 127432. https://doi.org/10.1016/j.jhazmat.2021.127432.
Sun, Q., He, J., Yang, H., Li, S., Zhao, L., & Li, H. (2017). Analysis of binding properties and interaction of thiabendazole and its metabolite with human serum albumin via multiple spectroscopic methods. *Food Chemistry, 233*, 190–196. https://doi.org/10.1016/j.foodchem.2017.04.119.
Tsirul'nikova, N. V., & Volkov, P. A. (2018). Synthesis of Polyacrylonitrile Fiber Aminated with Ethylenediamine in Aqueous Solution and the Vapor Phase. *Fibre Chemistry, 49*(6), 353–356. https://doi.org/10.1007/s10692-018-9899-x
Umapathi, R., Sonwal, S., Lee, M. J., Mohana Rani, G., Lee, E.-S., Jeon, T.-J., … Huh, Y. S. (2021). Colorimetric based on-site sensing strategies for the rapid detection of pesticides in agricultural foods: New horizons, perspectives, and challenges. *Coordination Chemistry Reviews, 446*, Article 214061. https://doi.org/10.1016/j.ccr.2021.214061.
Wan, M., Zhao, H., Wang, Z., Zou, X., Zhao, Y., & Sun, L. (2021). Fabrication of Ag modified SiO2 electrospun nanofibrous membranes as ultrasensitive and high stable SERS substrates for multiple analytes detection. *Colloid and Interface Science Communications, 42*, Article 100428. https://doi.org/10.1016/j.colcom.2021.100428.
Wang, K., Sun, D.-W., Pu, H., Wei, Q., & Huang, L. (2019). Stable, flexible, and high-performance SERS chip enabled by a ternary film-packaged plasmonic nanoparticle array. *ACS Applied Materials & Interfaces, 11*(32), 29177–29186. https://doi.org/10.1021/acsami.9b09746
Wang, Y., Li, P., Lin, D., Chen, J., Zhang, Y., & Yang, L. (2021). Ethanol-extraction SERS strategy for highly sensitive detection of poisons in oily matrix. *Spectrochimica Acta Part A: Molecular and Biomolecular Spectroscopy, 259*, Article 119883. https://doi.org/10.1016/j.saa.2021.119883.
Xu, J., Smith, S., Smith, G., Wang, W., & Li, Y. (2019). Glyphosate contamination in grains and foods: An overview. *Food Control, 106*, Article 106710. https://doi.org/10.1016/j.foodcont.2019.106710.
Yang, Y., Zhang, Z., He, Y., Wang, Z., Zhao, Y., & Sun, L. (2018). Fabrication of Ag@TiO2 electrospinning nanofibrous felts as SERS substrate for direct and sensitive bacterial detection. *Sensors and Actuators B: Chemical, 273*, 600–609. https://doi.org/10.1016/j.snb.2018.05.129.
Yu, Z., Wang, W., Kong, F., Lin, M., & Mustapha, A. (2019). Cellulose nanofibril/silver nanoparticle composite as an active food packaging system and its toxicity to human colon cells. *International Journal of Biological Macromolecules, 129*, 887–894. https://doi.org/10.1016/j.ijbiomac.2019.02.084.
Zhang, C., Yang, Q., Zhan, N., Sun, L., Wang, H., Song, Y., & Li, Y. (2010). Silver nanoparticles grown on the surface of PAN nanofiber: Preparation, characterization and catalytic performance. *Colloids and Surfaces A: Physicochemical and Engineering Aspects, 362*(1), 58–64. https://doi.org/10.1016/j.colsurfa.2010.03.038.
Zhao, Y., Yang, X., Pan, P., Liu, J., Yang, Z., Wei, J., … Liao, Z. (2020). All-printed flexible electrochemical sensor based on polyaniline electronic ink for copper (II), lead (II) and mercury (II) ion determination. *Journal of Electronic Materials, 49*(11), 6695–6705. https://doi.org/10.1007/s11664-020-08418-x
Zheng, S., Wang, Q., Yuan, Y., & Sun, W. (2020). Human health risk assessment of heavy metals in soil and food crops in the Pearl River Delta urban agglomeration of China. *Food Chemistry, 316*, Article 126213. https://doi.org/10.1016/j.foodchem.2020.126213.